ELSEVIER

Contents lists available at ScienceDirect

Journal of the European Ceramic Society

journal homepage: www.elsevier.com/locate/jeurceramsoc



Original Article

Ceramic materials and energy—Extended Coble's model and fractal nature



Vojislav Mitic^{a,b,*}, Goran Lazovic^c, Vesna Paunovic^a, Jih Ru Hwu^d, Shwu-Chen Tsay^d, Tsong-Ping Perng^e, Sandra Veljkovic^a, Branislav Vlahovic^f

- ^a University of Niš, Faculty of Electronic Engineering, Serbia
- ^b Institute of Technical Sciences of SASA, Belgrade, Serbia
- ^c University of Belgrade, Faculty of Mechanical Engineering, Serbia
- d Department of Chemistry and Frontier Research Center on Fundamental and Applied Sciences of Matters, National Tsing Hua University, Hsinchu, 300, Taiwan
- ^e Materials Science & Engineering Department, National Tsing Hua University, Hsinchu, 300, Taiwan
- f North Carolina Central University, USA

ARTICLE INFO

Keywords: Grains Pores Ceramics Micro-capacity Enthalpy Energy

ABSTRACT

The new frontiers open different directions within the higher and deeper knowledge structure using unemployed nano sizes domains. The BaTiO3 and other ceramic materials have fractal configuration nature based on three phenomena. First, ceramic grains have fractal shape looking as a contour in cross section or as a surface. Second, there is the so-called "negative space" made of pores and intergranular space. Third, there is fractal Brownian motion (fBm) within the material, during and after sintering, in the form of microparticle flow: ions, atoms, and electrons. Here, we took upon ourselves the task of extending Coble's model, with already generalized Euclidean geometries, by fractal nature correction. These triple factors make the very peculiar microelectronic environment electro-static/dynamic combination. The stress is here set on inter-granular micro-capacity in function of higher energy harvesting and storage. Constructive fractal theory allows identifying micro-capacitors with fractal electrodes. The method is based on the iterative process of interpolation which is compatible with the grain model itself. Inter-granular permeability is taken as the fundamental thermodynamic parameter function of temperature and enthalpy (Gibbs free energy), which are very important for a structure-energy relation.

1. Introduction

Ferroelectric materials, like ${\rm BaTiO_3}$ ceramic, have wide application in various electronic devices such as: transducers, actuators, multilayer capacitors, piezoelectric sensors, and memory. In the doped ${\rm BaTiO_3}$ ceramic, the influence of a certain dopant ion on electrical and dielectric properties depends on the nature of the compensation mechanism and location substitution in the perovskite structure. The undoped and the doped ceramic barium titanate has attracted considerable attention due to the possibilities of processing and design.

The main idea of this paper is to establish relations between the corrected and extended Coble's model of sintering and fractal nature material analysis, on one hand, and the ceramic materials and energy, on the other hand. So, we carefully develop the idea of the extended Coble's model. First, it is modelled on Euclidean geometry and, afterwards, a fractal nature analysis on this corrected model is conducted. All this is finalized with the fractal correction of temperature in the Gibbs free energy thermodynamic function, which is basically very important for new frontiers from the energy aspect in the ceramic

material science.

1.1. The Euclidean geometry approach

We have developed numerous methods for microstructure modelling grain geometry, grain boundary surface and contacts, which is essential for the optimization of electric and other properties. Most of these methods are based either on calculating contact surfaces in the prescribed volume of the ceramic sample or on defining shape modelling and contact surfaces by calculating values of the assigned two-grain model system geometry and the Euclidian geometry characterization.

1.1.1. The limitations of Euclidean geometry

The classic objects of Euclidean geometry are only idealized realworld abstractions and their use in modelling real phenomena and objects, which have a much more complex structure, are not always adequate and do not yield good results. Some of the examples include cloud formations, swirling water, the polarized light, the arrangement of stars in galaxies, vegetation, irregular forms of relief, the contours of

^{*}Corresponding author at: University of Niš, Faculty of Electronic Engineering, Serbia. E-mail address: vojislav.mitic@elfak.ni.ac.rs (V. Mitic).

the coastline, alveolar configuration of the lung tissues. In addition to the morphological sphere, noise in telecommunications, variation in different plants biomass and animal species or statistical performance of spoken language are functional sphere examples.

These objects, i.e. phenomena, have the following property in common: their structure is replicated and we will call such objects fractals. So, this is about the objects that possess the characteristic of self-similarity, each part of them is similar to the whole. How to describe objects with such a complex structure in the finite way? One of Euclidean geometry axioms states: The whole is greater than the part, thus Euclidean geometry fails to describe fractals as they are the objects whose proper part is equal (in some way) to the whole. Due to their complexity fractal objects cannot be described successfully without involving complexity.

However, some partial solutions appeared in the 1980s, these attempts were systematized by Benoit Mandelbrot.

1.1.2. Coble's model

The sintering consolidation is characterized by an extreme complexity due to the simultaneous and successive action of elemental mechanisms. Their qualitative and quantitative descriptions are very difficult [1-3]. Grain contacts are essential for understanding the complex electrodynamic properties of sintered materials [4]. The BaTiO3 and other ceramic materials, observed by the SEM method, are the characteristic example of complex shape geometry, which cannot be easily described or modelled. A possible approach for describing contact phenomena is the establishment of the grain contact models that would show that they have the highest influence on the electrical properties of the entire sample [5,6]. Intergranular contacts are formed during the sintering when powder particles form a contact, interatomic forces form a particle's neck, and there is a potential increase in the density of the aggregate. Transport mechanisms contribute to neck growth and densification. A common driving force is the reduction in the surface area and, thus, the surface free energy of the system reduction. A neck begins to grow controlled by different diffusion mechanisms (lattice and grain boundary diffusion, etc.) with the rates determined by the total flux of atoms coming to the neck. One of the goals of this paper is to establish the model of three or more spherical grains or otherwise-shaped grains in contact as a base for calculating possible contact area values in a given geometry configuration. This can be used in two ways: first, the simulation of neck growth in time domain can be done by combining results for the contact surface values with the kinetics of forming three or more contact areas; second, the model of three or more grains in contact can be used for establishing the equivalent electrical model of such grain clusters. A ceramic sample can be modelled as impedance, containing two capacitors, an inductor, and a resistor [7], and consists of numerous grains, organized in differentsized clusters. It could be assumed that each cluster and even intergranular contacts within the cluster - aggregates, show similar behaviour. The dominant contribution to the equivalent impedance within a wide frequency range comes from a capacitance [7]; intergranular contact can be observed as an intergranular micro-capacitor. Thus, all of these models and electrical contact surface processes are based on the application of modelling and simulation methods. Most of the models have used two spheres as the simplest, and, thus, the most convenient for studying, elemental mechanisms responsible for the progress of sintering process. Such an idealization of the particle geometry allows a very detailed study of the physical processes active in the contact region. In this paper, the Coble's two-sphere model [8] is used as the starting point for developing a new two-ellipsoid model that can approximate particles in a better way than the spherical one. The relations, connecting the geometric parameters of the ellipsoidal model with the parameters-sintering time and the temperature, are established. For the purpose of better understanding of intergranular processes, Coble's model was generalized for other possible grain shapes (sphere-polyhedron, polyhedron-polyhedron) and the new model

results are compared with those obtained from the two-sphere model. All calculations are valid for initial stage of the sintering process.

1.1.2.1. Modelling procedure.

- For spherical grain modelling the polyhedron-polyhedron model system is used.
- The surface of grain is represented by a series of polygons.
- Also, the belonging function is used for the representation of grain.
 It is a real function f(x, y, z) representing the grain as follows: an arbitrary point M(x1, y1, z1) belongs to the interior of the grain if f (x1, y1, z1) ≥ 0, and it is outside the grain if f(x1, y1, z1) < 0.
- Two grains are fixed in space so that they can touch or intersect with
 one another, and the third one is introduced along the determined
 direction. We have observed the process from the moment the mobile grain got into contact with one of the static grains until the
 moment the two grains assimilated the pore between them disappeared.
- During the simulation, the area of each contact surface, distance between each pair of grains, as well as the length of the pore formed between the grains have been calculated.
- The edge polygons are not treated due to their small influence on the value of the total area (less than 10-4 for the approximation of grain with 1,000,000 polygons) as well as considerable influence on the simulation rate.

1.1.2.2. The sphere-sphere model. With the aim of explaining a two-grain contact during sintering and better understanding of ceramic electrical properties, we start with the Coble's two-sphere model. In the initial-stage sintering diffusion process, two grains, approximated by spheres, penetrated each other slightly. The volume that fills the intersection of the spheres (the distance between centers is smaller than the sum of two radii) transforms into a neck (a kind of a collar that circumscribes the contact area). The starting model for the densification simulation during the initial sintering will be the Coble's two-sphere model (Coble, 1973), considered to be the volume conservation principle. According to the notation from the Fig. 2 a), we have relations:

$$\rho_1 = \frac{X_2^2}{4 \cdot R_1} \quad \rho_2 = \frac{X_2^2}{4 \cdot R_2} \quad X_2 = \sqrt{2} \cdot X_1 \tag{1}$$

where ρ_I , ρ_2 – the heights of spherical caps (forming the common volume of the sphere intersection), X_1 – radius of the common circle; X_2 is the radius of the neck formed by diffusion in initial stage of sintering, and R_1 and R_2 – radii of the two spheres.

In general case, the time dependent neck radius can be written in the form $x = g(t; T, \mathbf{A})$, where T is sintering temperature, and \mathbf{A} is the system parameter vector:

$$\mathbf{A} = \{a, \mathbf{D}, \mathbf{Q}, \gamma, T_m, \Omega, \delta_B\},\$$

where a is particle radius, D and Q are the diffusion coefficients vectors and the activation energies of transport mechanisms, respectively, – the boundary-free energy, – the melting temperature, \ast – the atom volume, and – the effective grain boundary thickness.

The next assumptions are: (i), (ii) the volume conservation, (iii) the center-to-center approach, and (iv) the straight-line neck geometry. Densification will be the result of the action of two possible transport mechanisms: the lattice and the boundary diffusion. For the model system topology shown on Fig. 2 e) f), Chen and Johnson (1989) in their extended model, equations for the lattice and the boundary diffusion of the following type:

$$Y_1 + Y_2 = [B_L t(\frac{1}{R_1} + \frac{1}{R_2})]^{1/2}, \ B_L = 8D_L \frac{\gamma \Omega}{kT}$$
 (2)

$$Y_1 + Y_2 = [B_B t(\frac{1}{R_1} + \frac{1}{R_2})]^{1/3}, B_B = 12D_B \delta_B \frac{\gamma \Omega}{kT}$$
 (3)

where and are the lattice and the grain-boundary diffusion coefficients, respectively.

1.1.2.3. The ellipsoid-ellipsoid and the grain-contact model. The ceramic sample grains can be approximated by ellipsoids scattered throughout the material's volume. The ellipsoids can be seen as a model of grains in contact. Actually, due to sintering pressure and sintering process, one grain partly penetrates into another, forming a small contact area that can be pretty accurately approximated by intersection of ellipsoids E_1 and E_2 . Our aim is to determine the value of this area as the function of the grains center distance δ_E .

We assumed that the ellipsoidal axes are pairwise parallel and lengths of the axes are proportional by the factor k. Consider two ellipsoids E_1 and E_2 , having centers at $C_1 = (x_1, y_1, z_1)$ and $C_2 = (x_2, y_2, z_2)$ from \mathbf{R}^3 , being coaxial (having parallel axes) with semi-axes a_i , b_i , c_i (i=1,2) provided that $a_i > b_i > c_i$, and $a_2/a_1 = b_2/b_1 = c_2/c_1 = k$ (k>0). Suppose that E_1 and E_2 approximate two neighbour grains in sintered ceramic (Fig. 2. b)). Straightforward calculation gives that the distance between C_1 and C_2 in the beginning of sintering (sintering time $\tau=0$) is given by

$$\delta_E^0 = \frac{1+k}{\sqrt{\frac{\cos^2 \alpha}{a_1^2} + \frac{\cos^2 \beta}{b_1^2} + \frac{\cos^2 \gamma}{c_1^2}}} \tag{4}$$

where $(\cos \alpha, \cos \beta, \cos \gamma)$ is the unit vector of C_1C_2 -segment. It is clear that $(1+k)c_1 \le \delta_E^{\circ} \le (1+k)\alpha_1$.

By the relations (1) from the Coble's two-sphere model ([3]) the difference between the grain center distances at the beginning and at the end of sintering during the elapsed time τ is given by

$$\delta(\tau) = \delta_E^0 - \delta_E(\tau) = \left[1 + \frac{X_2^2}{4 \cdot R_1^2 \cdot k} \right] \delta_E^0.$$
 (5)

The value of $\delta(\tau)$ contains information about dynamics of the intergrain neck formation and we can express the neck radius via the proportionality factor k as

$$X_2 = 2\mu \sqrt{\left(\frac{\delta_E^0 - \delta_E}{\delta_E^0} - 1\right)k},\tag{6}$$

where $\mu = R_1$ -the radius of spherical grain corresponding to ellipsoidal grain E_1 .

The presented model is tested for the case of two grains shown in Fig. 1b. According to the given micrograph ratio, the dimensions of grains are as follows: $a=3.1~\mu m,~b=2.7~\mu m,~and~c=1.3~\mu m.$ Since

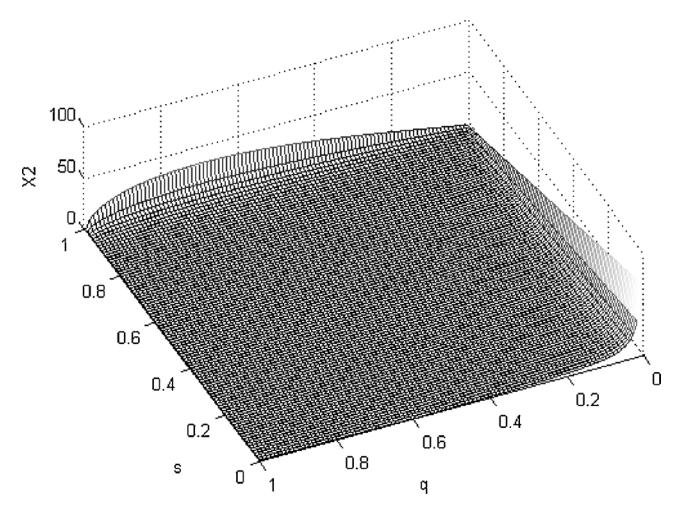


Fig. 1. Diagram of X_2 via $(d-R_2)/R_1$ and q.

the ellipsoids are coaxial, it is possible to close a Cartesian coordinate system having axes parallel to the axes of ellipsoids. Formula (3) can be put in the more explicit form

$$X_2 = 2\mu \sqrt{\frac{k\delta(\tau)}{k+1} \cdot \sqrt{\frac{\cos^2\alpha}{a^2} + \frac{\cos^2\beta}{b^2} + \frac{\cos^2\gamma}{c^2}} - k}.$$

If we apply the transformation inverse to (2) onto the circle of the interspherical contact of Coble's model we will get the elliptical area of the intergrain neck with the semi-axes X_2/b , X_2/a . The corresponding area is $A = X_2^2 \pi a^{-1} b^{-1}$.

By the formula (2) $X_2 = \sqrt{2}X_1$, where X_1 is given by

$$X_{1} = \sqrt{\frac{R_{1}^{2} + R_{2}^{2}}{2} - \frac{d^{2}}{4} - \frac{(R_{1}^{2} - R_{2}^{2})^{2}}{4d^{2}}}, R_{2} \le d \le R_{1} + R_{2},$$
(7)

where d is a distance between the sphere centers and $R_2 \ge R_1$. If we denote $q = R_1/R_2$, then, the neck radius will be given by

$$X_2(s) = R_2 \sqrt{1 + q^2 - \frac{(s-1)^2}{2q^2} - \frac{q^2(q^2 - 1)}{2(s-1)^2}},$$
(8)

where $s = (d-R_2)/R_1$. The formula (8) gives the relationship between the neck radius and the center sphere distance d normalized on the unit interval. The corresponding diagram is given in Fig. 1.

1.1.2.4. The sphere-polyhedron model. We suppose that a grain has approximately spherical shape but the roughness of the surface justifies replacing the spherical model with the polyhedral one. In order to describe a constructive way of obtaining such a polyhedron we will consider a specific subdivision procedure illustrated in Fig. 2d). Replace a sphere by a regular polyhedron inscribed in the sphere. Among five regular polyhedra, icosahedron is the best choice for two reasons. First, it is the best approximation of the sphere; second, all its faces are triangles which simplifies subdivision procedure.

Suppose that there are two grains, once approximated by an n-stage polyhedron (inscribed into a sphere having radius R_1) and another by a sphere (radius = R_2) (Fig. 2. e)); the two spheres penetrate each other for the same spacings ρ_1 and ρ_2 as in Fig. 2. a). After this, we need to evaluate the volume of the "cap" of n-stage polyhedron that contained in the R_2 - sphere. For this purpose, we will use the cubic function that shows the cap volume increase with the height ρ : $V_{\rm cap} = \pi \, \rho^2 (R - \rho/3)$. Finally, we get an approximate formula

$$(V_n)_{cap} = \frac{3 \cdot V_n}{R_1^3} \cdot \rho^2 \cdot \left(R_1 - \frac{\rho}{3}\right) \tag{9}$$

where $V_n=V_0\left[1+k+k\beta\cdot\frac{1-(k\beta)^{n-1}}{1-k\beta}\right]$ -polyhedron volume after n-steps, $\beta=\frac{\alpha}{1+k\alpha}$ and $\alpha=\frac{4\cdot\pi\cdot(3-\sqrt{5})-5}{5\cdot k}-1$. During the initial stage of the sintering process, two grains penetrate

During the initial stage of the sintering process, two grains penetrate each other and form a neck. The diameter of the neck is determined by the volume conservation law.

1.1.2.5. The polyhedron-polyhedron model. The importance of this model is in having a simple tool for manipulation and fast evaluation in the situation when we have a huge number of grains to process. Also, it can be used as a starting point for developing the fractal model of intergrain configuration. Here, we start with two polyhedra, P_m and P_n obtained as an m-stage or n-stage output of the above described procedure (Fig. 2. d)). So, we can use the formula (5) with R_1 and R_2 as the corresponding radii of the circumscribed spheres. The neck radius value depends on the parameters Vn, R_1 , R_2 , ρ , k, α , and β . Using this procedure, the geometry of two-polyhedral grains in contact can be successfully solved (Fig. 2. f)).

1.1.2.6. The spherical to ellipsoidal model transformation. The spherical model can be successfully converted into the ellipsoidal one by applying an affine transformation Φ : S \rightarrow E of the form

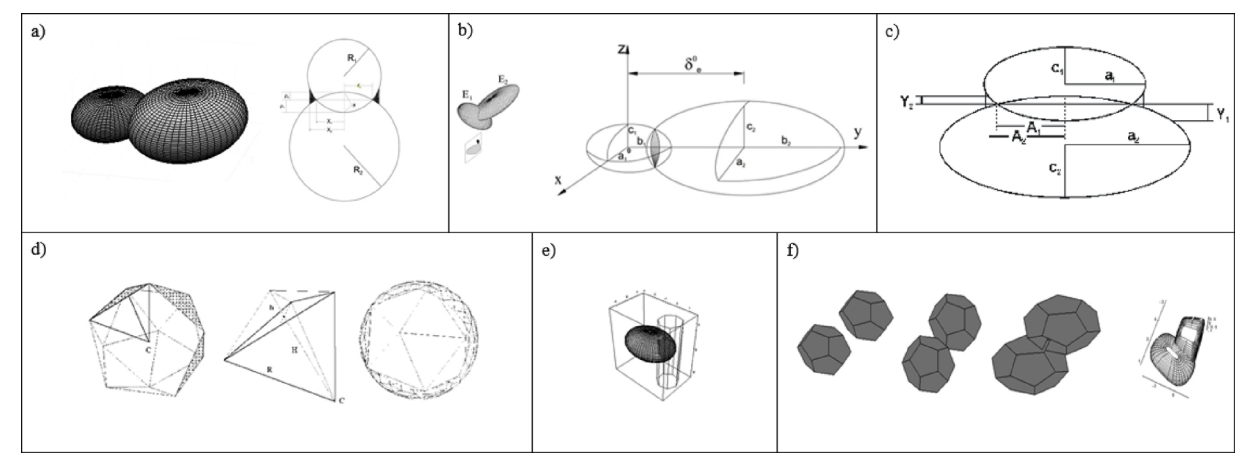


Fig. 2. a) The Coble's two-sphere model; **b)** The neck growth of two ellipsoidal grains in sintering process; **c)** The ellipsoidal model presented in *xOz* plane; **d)** The geometry of an icosahedron subdivision ellipsoid-polyhedron; **e)** The ceramic grains approximated by sphere-polyhedra penetration in sintering process; **f)** The polyhedron-polyhedron model system.

$$\Phi: \begin{bmatrix} x \\ y \\ z \end{bmatrix} \to \begin{bmatrix} x/a \\ y/b \\ z/c \end{bmatrix} (a, b, c > 0)$$
(10)

where a, b, and c are scaling parameters introduced in order to generate ellipsoidal semiaxes a_i , b_i , and c_i (i=1,2), while x, y, and z are local variables. The main properties of this transformation are its non-singularity (a, b, $c \neq 0$) and *continuity* which induces *topological invariance*. This means that the ratio conserving property of the transformation (4) is of essential importance for deriving the ellipsoidal model.

1.1.2.7. The new ellipsoidal model. Let E_1 and E_2 be two ellipsoids obtained from spheres S_1 and S_2 by introducing an affine transform (10) in the following way

$$\Phi: S_{1}(R_{1}) \to E_{1}(\frac{R_{1}}{a}, \frac{R_{1}}{b}, \frac{R_{1}}{c}) = E_{1}(a_{1}, b_{1}, c_{1})$$

$$\Phi: S_{2}(R_{2}) \to E_{2}(\frac{R_{2}}{a}, \frac{R_{2}}{b}, \frac{R_{2}}{c}) = E_{2}(a_{2}, b_{2}, c_{2})$$
(11)

The beginning assumption is that ellipsoids are "geometrically similar", i.e. their corresponding axes are parallel. Furthermore, let the centers C_1 and C_2 lie along the z-axis and $C_1 \neq C_2$. In such a case, transformation of the values ρ_1 and ρ_2 will be given as $\Phi: \rho_1 \to \rho_1/c$ and $\Phi: \rho_2 \to \rho_2/c$ (Fig. 2. c)).

After transform (11) is applied, the intersection circles of radii the X_1 and X_2 in the spherical model will be converted into the ellipses of the semi-axes A_1 , B_1 and A_2 , B_2 , respectively. The semi-axes A_1 and A_2 correspond to the x-axis, while B_1 and B_2 correspond to the y-axis. Thus, the new relations are established

$$\frac{X_1}{a} = A_1, \quad \frac{X_1}{b} = B_1 \quad \frac{X_2}{a} = A_2, \quad \frac{X_2}{b} = B_2$$
 (12)

In addition, we adopt Coble's model so that $R_2 = kR_1$ ($k \in R$) which gives the proportion

$$\frac{R_2}{R_1} = \frac{a_2}{a_1} = \frac{b_2}{b_1} = \frac{c_2}{c_1} = k, \quad (k \in \mathbb{R}). \tag{13}$$

Substituting the Eqs. (11) and (12) in (2), the volume conservation relations for ellipsoidal intersection are determined as:

$$\rho_1 = Y_1 = \frac{c_1 A_2^2}{4a_1^2}, \quad \rho_2 = Y_2 = \frac{c_1 A_2^2}{4ka_1^2}$$
(14)

or

$$\rho_1 = Y_1 = \frac{c_1 B_2^2}{4b_1^2} \quad \rho_2 = Y_2 = \frac{c_1 B_2^2}{4kb_1^2} \tag{15}$$

Similar expressions can be derived if coordinate system is set in a different way, i.e. approaching of ellipsoids is along x- or y-axis.

Considering ellipsoidal model, relations for lattice and boundary diffusion for approaching along z-axis, will be given now as

$$(Y_1 + Y_2)_z = \frac{1}{c} \left[B_L t \left(\frac{1}{cc_1} + \frac{1}{cc_2} \right) \right]^{1/2}, \tag{16}$$

$$(Y_1 + Y_2)_z = \frac{1}{c} \left[B_B t \left(\frac{1}{cc_1} + \frac{1}{cc_2} \right) \right]^{1/3}. \tag{17}$$

Similar expressions can be generated for approaching along x- or y-axis. By substituting relations (14) or (15) in (16) and (17) ellipsoidal model for determination of grain growth kinetics during the initial stage of sintering $(A_2 = f_n(t, T))$ and $B_2 = f_n(t, T)$ are established.

1.1.2.8. The extended and corrected Coble's model. Coble's model deals with spherical approximations of grains. This model can be extended to more natural models where two neighbour grains are replaced by two ellipsoids E_1 and E_2 given by

$$E_{1}\begin{bmatrix} x(\theta,\phi) \\ y(\theta,\phi) \\ z(\theta,\phi) \end{bmatrix} = R_{x}R_{y}R_{z}\begin{bmatrix} x_{1} + a_{1}\cos\theta\cos\phi \\ y_{1} + b_{1}\cos\theta\sin\phi \\ z_{1} + c_{1}\sin\theta \end{bmatrix},$$

$$E_{2}\begin{bmatrix} x(\theta,\phi) \\ y(\theta,\phi) \\ z(\theta,\phi) \end{bmatrix} = R_{x}(\theta_{x}^{\prime})R_{y}(\theta_{y}^{\prime})R_{z}(\theta_{z}^{\prime})\begin{bmatrix} x_{2} + a_{2}\cos\theta\cos\phi \\ y_{2} + b_{2}\cos\theta\sin\phi \\ z_{2} + c_{2}\sin\theta \end{bmatrix}.$$

The simple geometric argument says that two ellipses will touch each other provided that $P \equiv S$ and Q, R, T are collinear (Fig. 3. a)). The distance between the ellipse centers represents the distance between the grain centers at the beginning of the sintering, $\delta_E(\tau=0)$ and is given by

$$\delta_{E}(\tau=0) = \sqrt{\frac{p_{1} + r_{1} - 2q_{1}\omega_{1}^{2}}{2(1 - \omega_{1}^{2})} + \frac{s_{1} + u_{1} - 2t_{1}\omega_{2}^{2}}{2(1 - \omega_{2}^{2})}}^{2} + \left(\frac{p_{2} + r_{2} - 2q_{2}\omega_{1}^{2}}{2(1 - \omega_{1}^{2})} + \frac{s_{2} + u_{2} - 2t_{2}\omega_{2}^{2}}{2(1 - \omega_{2}^{2})}\right)^{2}}$$

After the sintering is completed, the grains partially penetrate each other and the distance shrinks to $\delta_E(\tau \neq 0)$ (Fig. 3 b), c)).

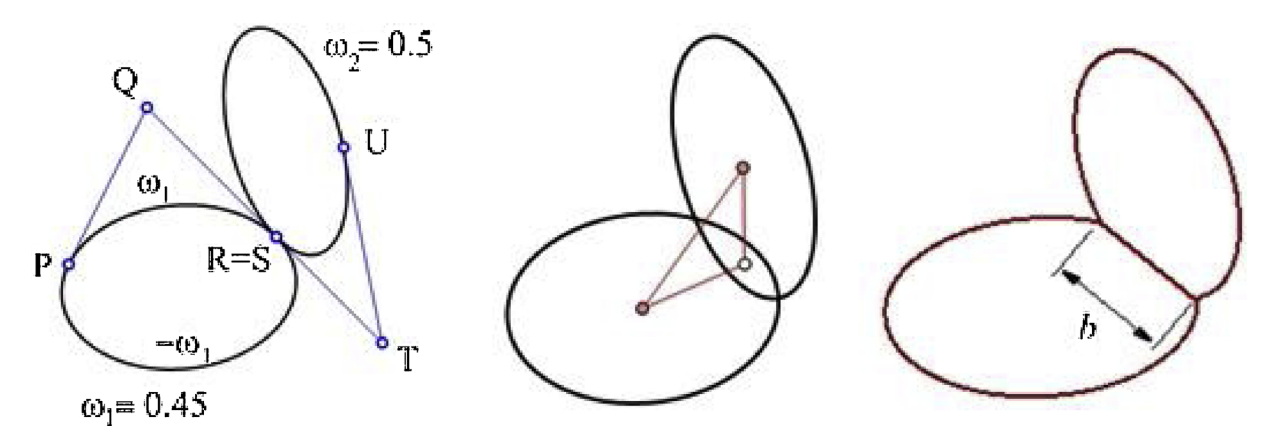


Fig. 3. Ellipsoid cross section: a) Touch of two grains; b) grains partially merged;c) the touching surface and one of its linear dimensions.

1.2. Fractal intro

The most important term in the theory of fractals is first established by Benoit Mandelbrot in [21,22]. The explanation of the role of fractal dimension will be elaborated below.

The fractals are geometric objects of a broken, fragmented, wrinkled, or amorphous form or being highly irregular in some other way. The standard Euclidean geometry fails to describe such objects so that they are the subjects of fractal geometry. The term fractal, as a neologism derived from the Latin adjective word "fractus", is defined as a broken or shattered stone. The more irregular the stone the higher the fractal dimension. In fact, Hausdorff dimension or fractal dimension DH_f is a real number to the contrast of usual notion of dimension which is called topological dimension DT (DT = 0 for isolated points, DT = 1 for curves, DT = 2 for surfaces, DT = 3 for solids, etc.). So, Hausdorff dimension $0 < DH_f < 1$ covers all objects that are more than a point but less than a curve.

The typical example is the Cantor set with $DH_f = \ln 2/\ln 3 \approx 0.6309$. If $1 < DH_f < 2$ the object is something between the curve and the surface, with famous Sierpinski triangle having fractal dimension $DH_f = \ln 3/\ln 2 \approx 1.5849$. However, the Cantor set and the Sierpinski triangle are mathematical constructions. Direct analogy to the Cantor dust is fine particle dust - the dust that floats in the air. Brian Kaye devoted the whole part (Part 3.7 of [1]) to the fractality of different dusts: mine dust, coal dust, fumed silica, shellac droplets, radioactive dust, welding dust, and, finally, powders for ceramic industry. Speaking of fractal objects with fractal dimension between 1 and 2, a nice example are coastlines. The coastline of Ireland has been reported to have fractal dimension of approximately 1.22, the coast line of Great Britain is 1.25 and the coast line of Norway is the most irregular one with $DH_f \approx 1.52$. Since the maritime coasts are just level lines of geomorphic relief formations, the same can be applied to ceramic grains. So, there is a reason to study the contours of grains which are more or less complicated lines. Finally, the BaTiO3-ceramic grains as 3D objects have fractal surfaces which means that their fractal dimension is the real number between 2 and 3. Theory shows that any surface generated by regular Brownian motion has $DH_f = 2.5$ which is the same as fractal dimension of crumpled paper. Just for comparing, DH_f for cauliflower surface is 2.33, for human brain 2.79 and for human lungs 2.97.

The concept of Iterated Function System (IFS) and its affine invariant counterpart AIFS appear to play a crucial role in the constructive theory of fractal sets and in paving the way to having a good modelling tools for such sets. If the collection of objects to be modelled, besides fractals, contains smooth objects as well (polynomials, for example), then, one needs to revisit classical algorithms for smooth objects generation and introduce the new one that is capable of creating both the fractal and the smooth forms. In this light, and following the problem from the Barnsley book [13], the purpose of this paper is to

develop such algorithms for interpolating polynomials.

Let $\{w_i, i = 1, 2, ..., N\}$, $N \ge 2$, be a set of contractive affine mappings defined on the complete Euclidian metric space (R^m, d_E)

$$w_i(x) = \mathbf{A}_i x + \mathbf{b}_i \quad x \in \mathbb{R}^m, \quad i = 1, 2, ..., n$$

where A is an $m \times m$ real matrix and b is an m-dimensional real vector.

The mapping w is "contractive "if it maps the bounded original set into set that is "smaller "in the sense of the Hausdorff metric. The fractal A is a subset of the complete metric space, which is invariant in relation to the union of contractive W mappings, i.e. W(A) = A. Thereupon, the Hausdorff dimension of this subset DH(A), as a rule, is a noninteger real number.

1.2.1. Intergranular connections

1.2.1.1. The fractal capacity corrected Heywang model. Grain contacts are essential for understanding the complex electrodynamic properties of sintered materials. BaTiO3-ceramic microstructures obtained by SEM are typical examples of a complex shape geometry which cannot easily be described or modelled. A possible approach for describing contact phenomena is establishing the grain contact models. Our new approach includes fractal geometry in describing the complexity of the electroceramic grain spatial distribution. Modelling method allows the presentation of grains in contact within the sphere, ellipsoid, and polyhedron shape. In spherical and the ellipsoidal grain model systems there is a possibility for the analytic expressions of grain shape and contact surface, presented as the functions of distance between grains. On the other hand, the polyhedron-polyhedron model presents the real numerical procedure. Here, each grain is approximated by an ellipsoid. Also, it can be expected that the contact zone has ellipsoidal geometry as well. The contact surface between two grains must also inherit a trace of ellipsoidal geometry. However, this surface can be approximated by an ellipse having semi-axes X/b, XIa. This means that the contact surface area between two grains, after sintering, should be approximately

$$A_S = \frac{4\pi R^2 k}{ab} \left(\frac{\delta(\tau)}{\delta_E^0} - 1 \right)$$

Due to diffusional forces that appear in the sintering process we are ready to believe that an approximate form of a contact surface is the shape of a minimal surface – the surface with a minimal area size. Nevertheless, the microstructure of the material makes this surface a fractal locally (Fig. 4).

Considering that intergrain contact surface is the region where processes occur at the electronic level within the electroceramic material, structural complex grain contact-grain can be represented by an electrical equivalent network consisting of three RC branches. The contact between two grains is observed as planar microcapacitor. The surfaces of capacitor plates correspond to the intersecting surface S of

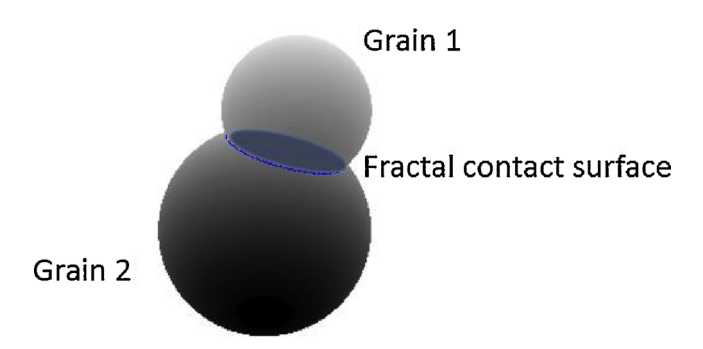


Fig. 4. An intergrain contact surface has a fractal form.

two grains. By applying the fractal approach to the intergrain geometry, the formula for the microcapacity of an intergranular condenser seen as a planar condenser is given into the following form

$$C = \varepsilon_0 \varepsilon_B \alpha \cdot \frac{S}{x} = \varepsilon_0 \varepsilon_B (N\xi^2)^k \cdot \frac{S}{x}$$
(18)

where ε_0 , ε_B are dielectric constants in a vacuum and in BaTiO₃-ceramic material respectively; S – the area of the "plates" and the x – distance between the condenser "plates", i.e. the condenser thickness and $\alpha = (N\xi^2)^k$, is a correction factor obtained through a constructive approach to the fractal surface. This approach uses an iterative algorithm that iterates the N self-affine mappings with a constant contractive (Lipschitz) factor $|\xi| < 1$ k-times³. The underlying theory and techniques for choosing the appropriate mappings are given in the previous work. Typically, $\alpha = D - D_T$, where $D \approx 2.08744$ is the fractal (Hausdorff) dimension of intergrain contact surface and $D_T = 2$ is the topological dimension of the surface. As it is found, the ceramic contact surfaces are of low-irregularity which is characterized by the small difference D- $D_T \approx 0.08744$.

The derived formula (18) indicates the increase of the value of microcapacity when fractal approach is applied. Thus, a more accurate calculation of microcapacitance generated in grain contact can be carried out leading to a more exact estimation of dielectric properties of the whole sample.

All this allowed us to consider the ceramic sample as a system with a huge number of clustered grains that are in contact with one another. For each of them, it is possible to establish the equivalent electrical model and, for a defined set of input parameters, by using a symbolic analysis, obtain the frequency diagram. However, the simple RC is not sufficient to explain resonant behaviour of a ceramic sample. In order to calculate the equivalent impedance for a wide frequency range, the equivalent electrical circuit for a ceramic material can be introduced as an impedance, containing two capacitances C and C_p , the inductance L, and the resistance R. Therefore, it is more likely that the equivalent circuit model of contacted grains has parallel and series branches as presented in Fig. 6. Two grains in contact, approximated by ellipsoids, are shown in Fig. 5.

In this way a ceramic sample can be considered as a huge heap of randomly scattered ellipsoids throughout the sample volume. What is interesting is to determine what the distribution of the intergranular contacts looks like. Secondly, what is a more general formula for evaluating the size of all contact patches in the ceramic volume unit. Finally, the most complex question is that of the nature of intergrain layers and their relationship with the microcapacitor distribution. Of course, it must be kept in mind that all parameters mentioned are the functions of sintering parameters (T, P and τ).

In the light of the geometric method explained above, we can extend this approach from the case of the EE intersections to the case of the EP and the EG intersections. In fact, the value of the two-grain contact area is given by

$$A = \int_{S} d\sigma \tag{19}$$

where S is a mathematical surface that will be described soon and do is a usual differential element of the surface. For all three models the surface S can be characterized in the unique way by the intersection of the ellipsoidal surface with: 1. another ellipsoidal surface; 2. the polyhedron surface; and 3. the real grain surface that can be expressed in terms of fractal functions. Even if the analytical method could be applied (EE), there would be no use for this because the evaluation method of the above integral must be a numerical one. Consequently, the method of two surface intersection is reasonable to be numerical, as well. In all cases, it is enough to find discrete points along the intersection line. In the case of EE intersection the analytical solution of the intersection is to be discretized which reduces the problem in the case of the EP intersection. The method is as follows:

The polyhedron P can be regarded as the union of the vertices V and the sides σ . The set of vertices is divided by the ellipsoidal surface E in two groups: V_1 – vertices inside of E including the surface; V_2 – vertices lay outside of E. These two groups of vertices divide the set of sides in three groups: $\sigma = \sigma_1 \cup \sigma_2 \cup \sigma_3$, where σ_1 are the sides whose both endpoints are in E; σ_3 are the sides outside of E; and σ_2 contains all sides that connect the vertices from V_1 with the vertices from V_2 . Each side from σ_2 contains a unique point being characterized by the unique parameter t, $t \in (0,1)$ so that $(1-t)\mathbf{p_1} + t\mathbf{p_2}$ is a point on the ellipsoid. If the ellipsoid has the semi-axes \mathbf{a} , \mathbf{b} , \mathbf{c} and $\mathbf{p_1} = (x_1, y_1, z_1)$, $\mathbf{p_2} = (x_2, y_2, z_2)$, the parameter t must obey the quadratic equal \mathbf{a} and \mathbf{a} has \mathbf{a} be \mathbf{a} be \mathbf{a} and \mathbf{a} has \mathbf{a} be \mathbf{a} be \mathbf{a} be \mathbf{a} by \mathbf{a} and \mathbf{a} has \mathbf{a} be \mathbf{a} be \mathbf{a} be \mathbf{a} be \mathbf{a} . The parameter \mathbf{a} is \mathbf{a} by \mathbf{a}

What we want to get is the ellipsoid-immersed P surface size value. Let this surface be denoted by π , then $|\pi|$ – the value we want – can be approximated by the union of triangular elements. The size of each triangle is given by the 1/2 of its sides' vector product modulus.

As far as the EG contact is concerned, the calculation is a little bit complex, mainly due to the fact that the fractal grain is defined by recursive functions (the fractal structure of such contact is shown in magnified detail in the scope of Fig. 6). However, using the binary tree algorithm and the convex hull property of fractal algorithms, the intersection of one meridian line in fractal grain with an ellipsoid is not difficult to find. Actually, let S_0 be a starting set in 3D space for the recursive procedure of making the autocomposition of the Hutchinson contractive operator. Then, a sequence of sets has been produced. Being a union of smaller copies of the attractorlet from the previous stage, the

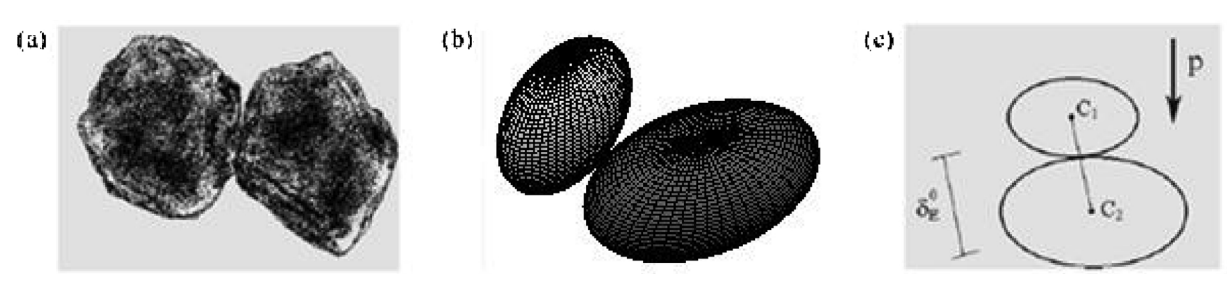


Fig. 5. a) two-grain real microstructure contact, b) and c) two grains in contact according to the ellipsoid-ellipsoid model.

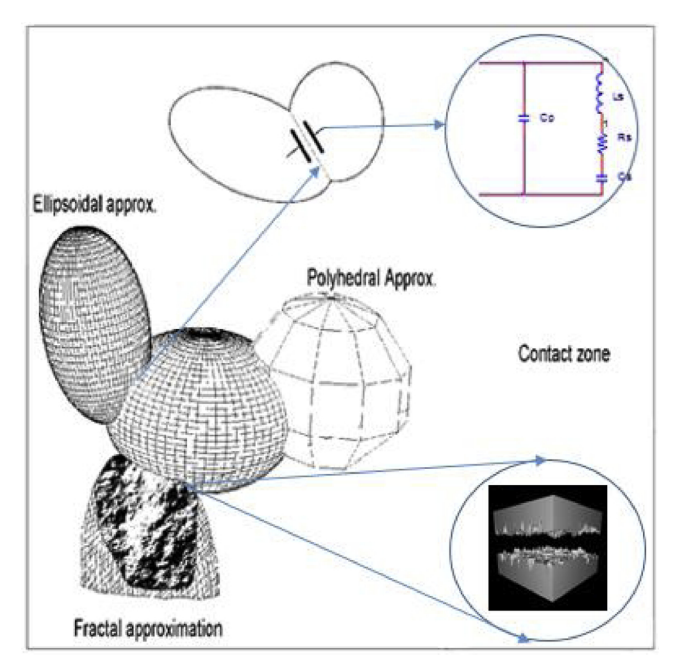


Fig. 6. The Ee-Ep-Eg-Group of *BaTiO*₃-ceramic grains and the fractal structure of the contact zone electrical equivalent model of contacted grains.

actual attractorlet obeys the convex hull property which allowed to find its intersection in any compact set in 3D. After the fractal intersection contour is determined, its area can be estimated by using the suitable numerical method.

The surface S that appears in the integral formula is the union of all intergrain contact surfaces in the prescribed volume V of a ceramic sample.

Let G be a contact zone between any two grains and $\chi_G(x) = \begin{cases} 1, & x \in G \\ 0, & otherwise \end{cases}$ characteristic function of the set G. Define the following function

$$F(x, y, z) = \chi_G(\mathbf{r}), \mathbf{r} = [x \ y \ z]^T \in \mathbf{R}^3$$

It is clear that F is a discontinued function defined over the volume of the considered sample. Let ∇F be the usual gradient of the function F with the convention that in the point of discontinuity r_0 , where the limes of pregradient fraction goes to infinity, it will be taken that $\nabla F(r_0) = +\infty$. It is easy to see that the set defined by $\partial G = \{r\colon |\nabla F(r)| > 1\}$ represents the surface of the A contact zone. In order to extend ΔG on all contact surfaces it is enough to replace the function F defined above by F_1

$$F_1(x, y, z) = \prod_{i \in I} \chi_{Gi}(\mathbf{r})$$

where I is a subset of a natural numbers broad enough to number all contact zones. The corresponding surface is $S = \partial G_1$ defined by

$$\partial G_1 = \{ \mathbf{r} : |\nabla F_1(\mathbf{r})| > 1 \}.$$

Therefore, the total contact area is given by

$$A = \int_{S} d\sigma = \int_{V} \prod_{i \in I} \chi_{Gi}(\mathbf{r}) d\sigma.$$

In the special case, when the grains are approximated by ellipsoids with parallel axes, the formula for A becomes a finite sum of all contact surfaces between grains. If two grains in contact are labelled by i and j, with the analogue meaning of $a_i b_j R_{ij}$ and k_p as above, the contact surface A_{ij} will be given by

$$A_{ij} = \frac{4\pi}{a_i b_j} R_{ij}^2 \frac{\max\{a_i, b_j\}}{\min\{a_i, b_j\}} \left(\frac{\delta(\tau)}{\delta_E^0} - 1\right),$$

which reduces (19) to $A = \sum_{ij} A_{ij}$..

2. Experimental

The samples used in our paper were prepared using the conventional solid-state reaction. As the starting powder it was used $\rm BaTiO_3$ (Murata) doped with different additives in concentrations ranging from 0.5 to 5.0 wt%. Starting powders were ball milled in ethyl alcohol, drying for several hours, and pressed into pellets at pressures ranging from 90 to 120 MPa. The pellets were sintered in air from 1,250 °C to 1,380 °C for 2 and 4 h. The microstructure was investigated using the scanning electron microscope, JEOL, SEM-5300 equipped with the EDS (Energy Dispersive Spectrometer) system. The electrical characteristics were measured using LCR meter Agilent 4284 A. The microstructures have been done with a selection of some grains and pores with minimum five magnifications because of the fractal nature analysis.

2.1. The microstructure fractal dimension and analysis

Based on several microstructures (different pressure, sintering time, and temperature) at different magnifications, we successfully performed the perimeters and grain shape reconstruction using the fractal nature analysis. Also, we are estimating the fractal dimension from these microstructures (Figs. 7–11)

The microstructure fractal nature analysis evidently opens new possibilities in the field of fractal microelectronics. In this sense, and enlightened by fractals, the grains and pores, microsurfaces, and shapes with their profiles are very important for developing new ideas for further miniaturization where the supermicro fractal contacts from different sides of each two grains are basic. The supermicro fractal capacitors practically connect fractal microstructure characteristics with electronic properties and also, even supermicro impedances, which could set a course for new research.

3. Results and discussion

3.1. The grain shape and the fractal analysis

Electroceramics, especially BaTiO3-ceramic, are made out of very fine powder having maximum Ferret diameter $D_{F \max} < 2 \mu m$. These particles have such a high surface energy to fuse together and make sintered ceramic. As Brian Kaye quotes in his pioneering book [1], many powder materials also have fractal structure. In fact, since the powder material is porous, there are two aspects of fractality: the positive space made of a grain collection and the negative space which is the collection of holes and pores. The ceramic material, during sintering, changes its inner morphology by shrinking pores and increasing its solidity and compatibility. Nevertheless, it still contains residual pores as it is also noticed in [1] where the sintered compact is shown to have holes and fractal structure found as we can see from the illustration in [2]. Researches concerning fractal properties of BaTiO₃ were first conducted in [3] and continued throughout a series of papers [3-19]. There, it was proven that several issues of fractality emerge in BaTiO₃ceramic:

- i The ceramic grain itself is a fractal object with irregular surface;
- ii The intergranular zone with different levels of grain contacts;
- iii The distribution of grains through the ceramic bulk also has a fractal character;
- iv The morphology of pores is a "negative space" fractal;
- v The dynamics of particles, adatoms, flows in a liquid sintering phase, and electrons behave as free particles performing Brownian walk which is known as an example of authentic fractality.

First of all, these elements contribute in energy distribution and energy transformation within the BaTiO₃-ceramic and consequently in

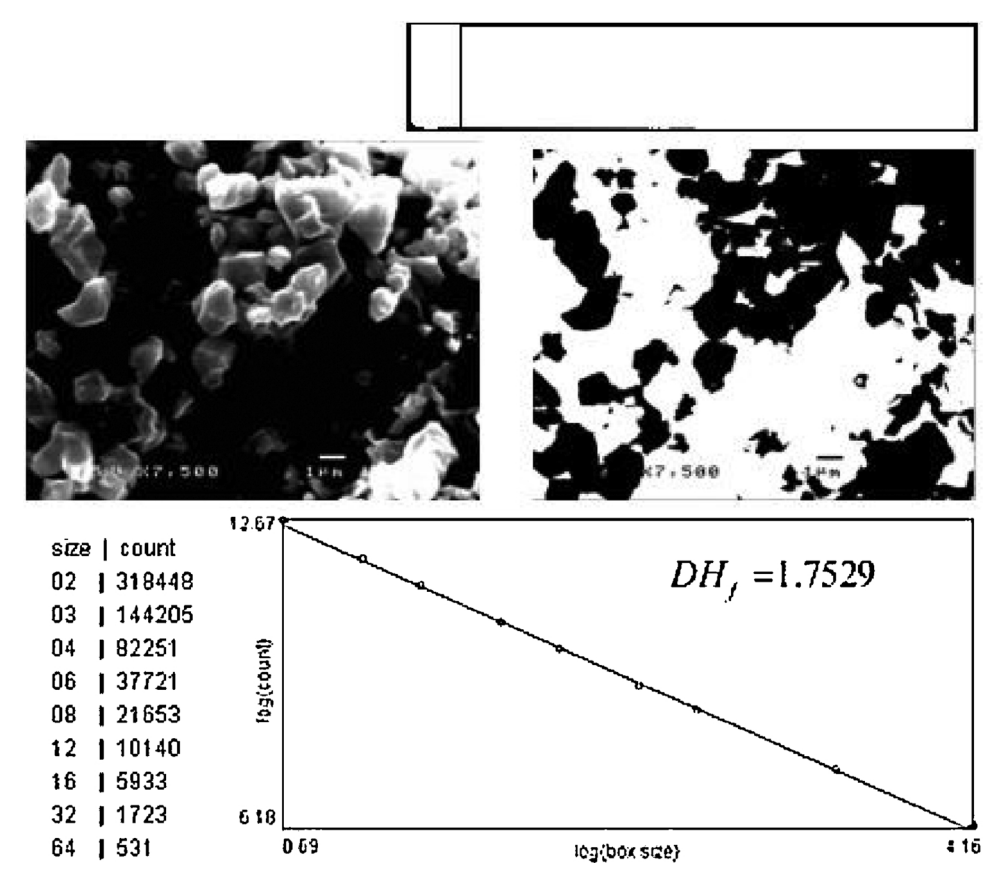


Fig. 7. The SEM sample (0.5 wt% Ho2O3) A1 sintered on $1320\,^{\circ}$ C and its fractal dimension extracted by a gray level box (24/255) counting $DH_f=1.7529$.

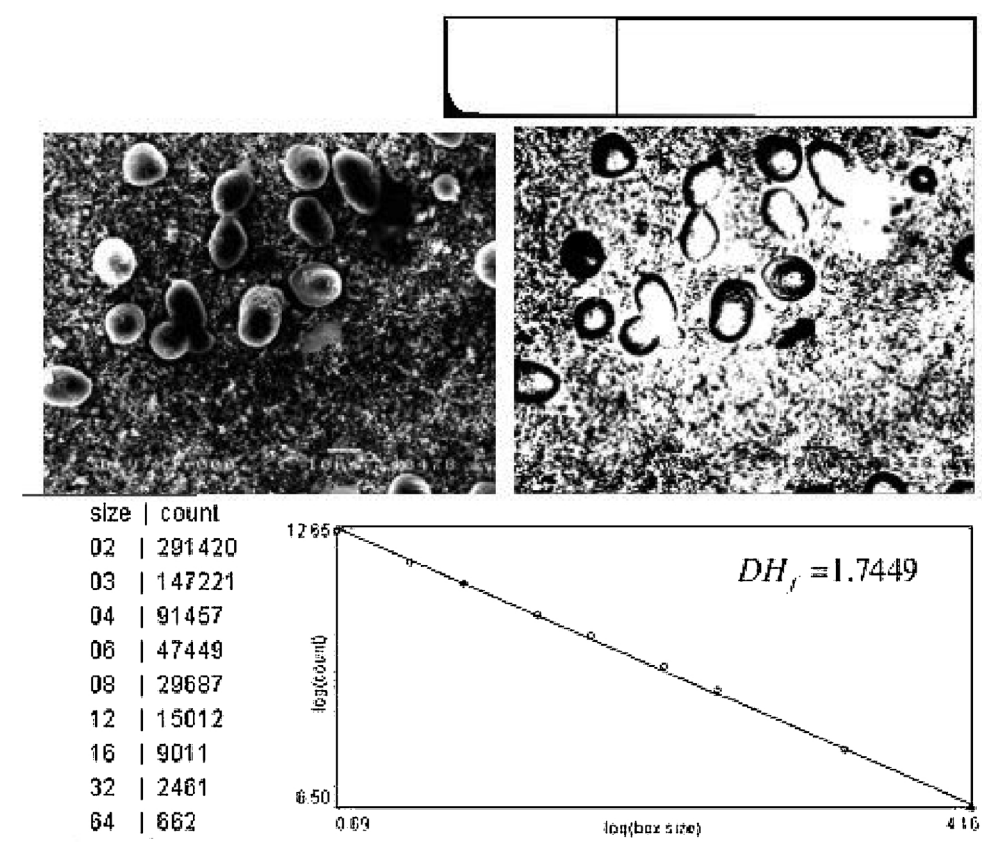


Fig. 8. The SEM of the sample (0.5 wt% Ho2O3) A2 sintered on 1320 °C and its fractal dimension extracted by gray level (83/255) box counting $DH_f = 1.7449$.

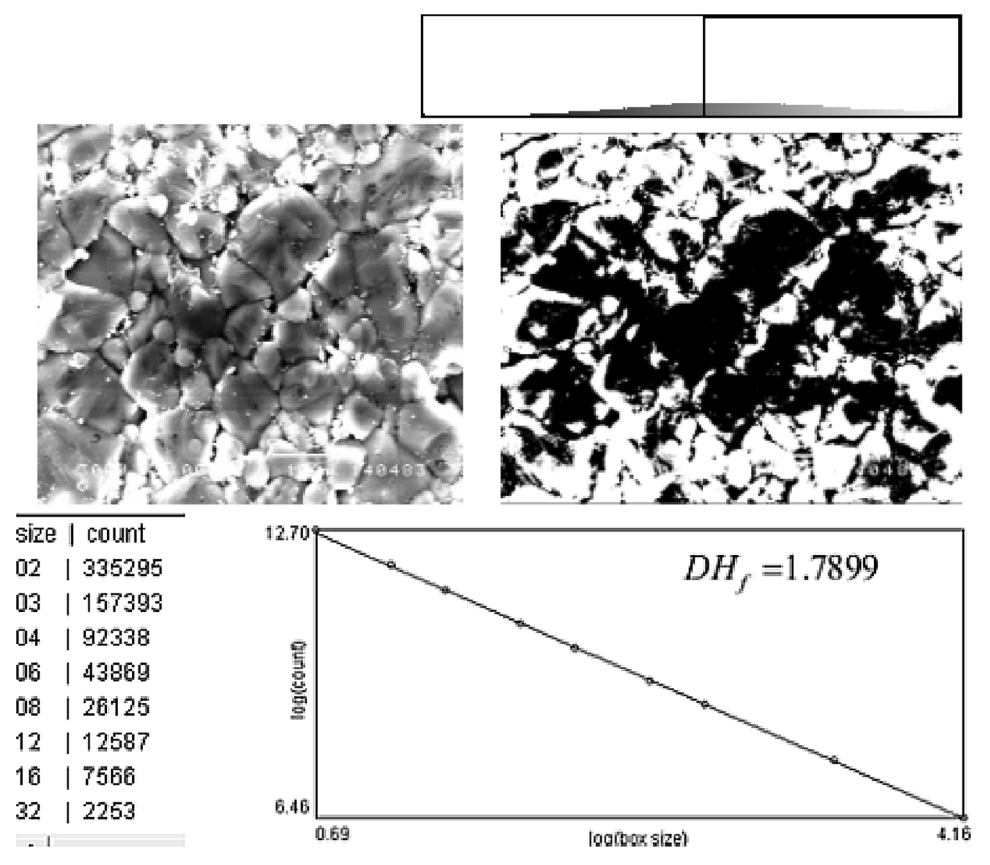


Fig. 9. The SEM of the sample (0.5 wt% Ho2O3) B1 sintered on 1380 °C and its fractal dimension extracted by gray level (134/255) box counting $DH_f = 1.7899$.

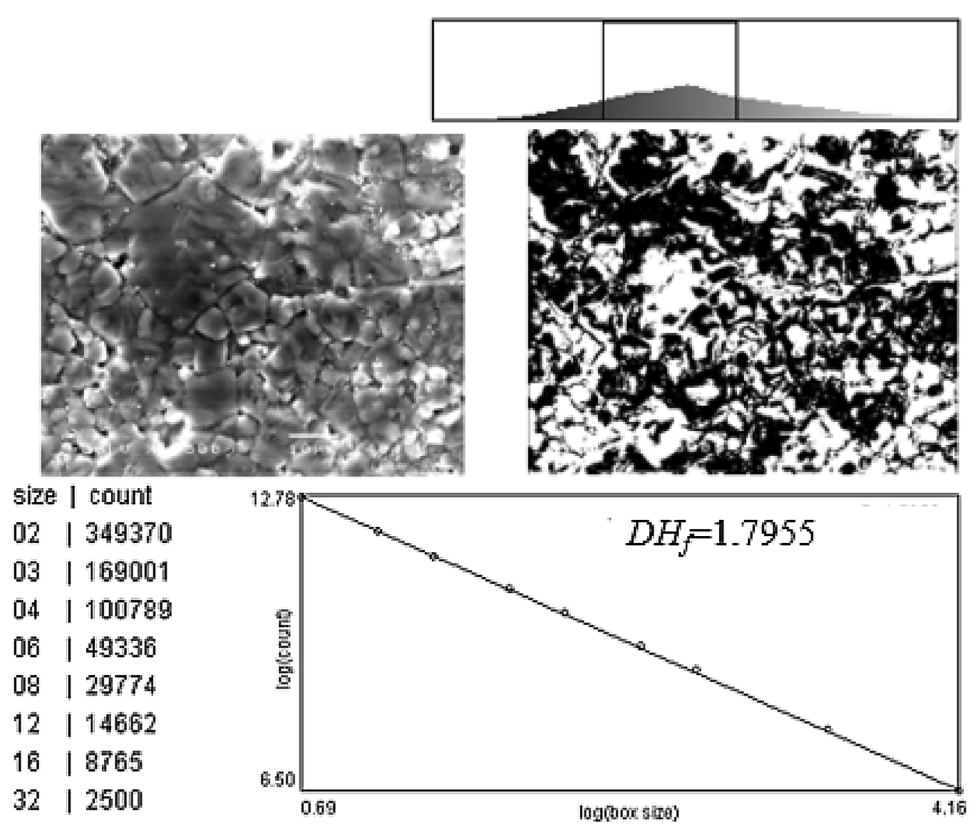


Fig. 10. The SEM of the sample (0.5 wt% Ho2O3) B2 sintered on 1380 °C and its fractal dimension extracted by gray level (83/148) box counting $DH_f = 1.7955$.

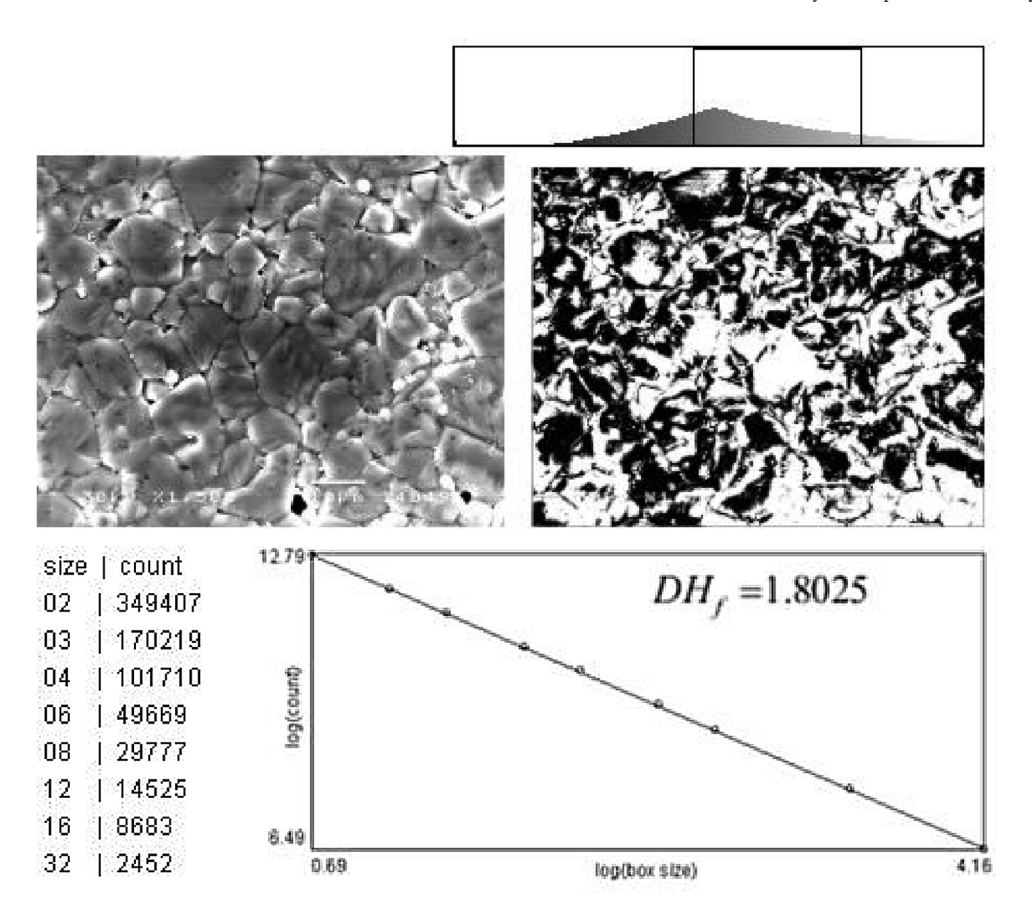


Fig. 11. The SEM of the sample (0.5 wt% Ho2O3) B3 sintered on 1380 °C and its fractal dimension extracted by gray level (116/197) box counting $DH_f = 1.8025$.

all dielectric, ferroelectric, PTCR, and piezoelectric phenomena. Recent investigations of Zheng et al. in [20] clearly show that the dielectric permittivity ε' and the piezoelectric constant d_{33} , for both poled and unpoled BaTiO₃-ceramic, increase significantly at room temperature with the reduction of the average grain size which is equivalent to the increase of *fractal dimension*.

Here, we present the new results concerning the doped $BaTiO_3$ -ceramic surface fractal dimension using the SEM micrographs. The samples that are used are: A1 and A2 and B1, B2, and B3, all at the same pressure of 120 MPa and for 4 h.

The procedure used is as follows: the grey microphotographs are converted to the black and white form using the given threshold or the levels ranging from 1 to 256. For all the levels, the box counting method is performed and the maximal result is set to output. The argument is obvious. The level that gives maximal fractal dimension is the one that reveals the most details. This means that we used modification of the classic box counting and employed the formula

$$DH_f(t) = \lim_{n \to \infty} \frac{\ln N_{\max}(2^{-n})}{\ln 2^n} = \frac{1}{\ln 2} \lim_{n \to \infty} \left(\frac{1}{n} \ln N_{\max}(2^{-n}) \right)$$
(20)

where $N_{\max}(\varepsilon)$ denotes the maximum number of boxes that contain black pixels upon the prescribed resolution ε , with the usual setting $\varepsilon=2^{-n}$, where n is the picture subdivision degree. This means that for n=1 the picture rectangle is not yet subdivided. For n=2, the rectangle is subdivided into 4 similar subrectangles by two lines passing through the middle points on the opposite sides. For n=3, the same subdivision is applied to each fourth of the rectangle, and so on. After n-th subdivision, one has 2^n subrectangles.

Also, on Fig. 12, we provide an example, for the sake of clarification, the 3D surface representation as the application of the previously described method. It is evident that 3D reconstruction of the grains and pores, corresponds to the SEM results on Fig. 7.

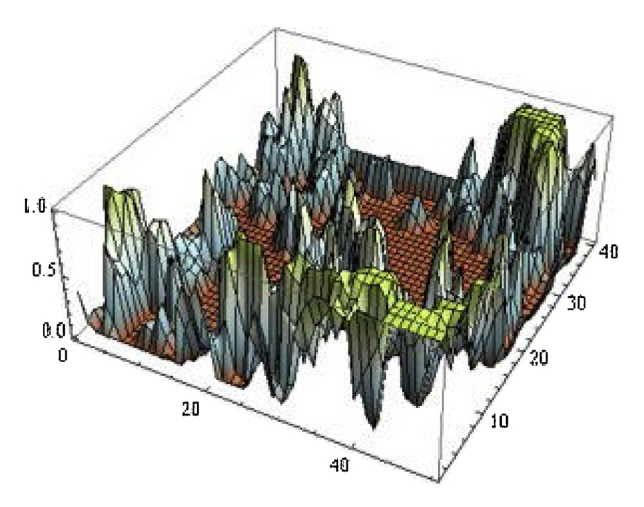
We strongly stress that the numerical result we may get using the formula (20) is a dimension of the picture we got from the SEM and not of the sample itself. So, it may differ from the real fractal dimension as much as the picture differs from the original. Also, it must be taken into account that the automatic counting boxes may also introduce some "numerical noise" as well as that the last square approximation also has its inherent error. However, in spite of this, the results are quite usable for comparing two different samples and are not an obstacle in gaining insight into the complicated processes of sintering and the electronic properties of consolidated materials (Fig. 13).

Each figure Figs. 8–12., in its upper part, gives the data of the sample and displays small diagram of grey levels. In the middle, the grey-shaded SEM photo and its B/W version (max level) are displayed. Finally, the lower part features numerical data obtained in box-counting and the log-log last squares fitting line which contains the approximate fractal dimension.

As it is evident from Table 1, the SEM microphotographs fractal (Hausdorff) dimension differs significantly for the A and B samples. Note that both the BaTiO $_3$ -ceramic samples were consolidated under the same conditions (additives, pressure, and sintering time) but at different temperatures. A higher temperature (1380°C) results in denser ceramic that is supposed to have a bigger fractal dimension. Our experiment confirms this statement. In fact, the temperature difference of 60°C results in the fractal dimension difference of 0.04407. Expressed in percentage, the temperature increment for 4.3% yields the 2.45% fractal dimension increment.

Looking back at our earlier research ([3–19]), we may observe several BaTiO₃-ceramic fractality "sources" as it is anticipated by the points i. to ν . in the section 3.1.

Also, it is worth mentioning that no research has been conducted in regard to the estimation of fractality in the field of ceramics. So, bearing in mind the mentioned limitations, this is what we now know about



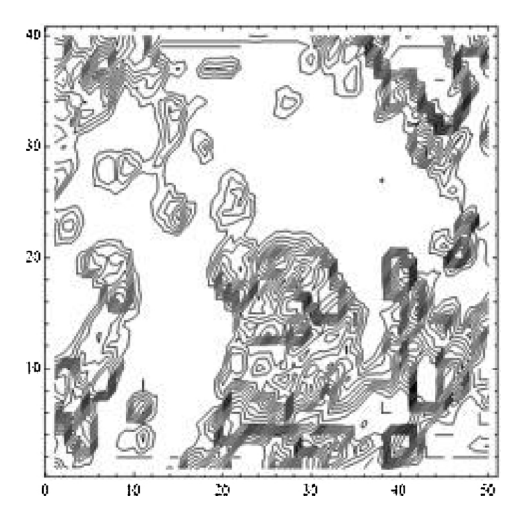


Fig. 12. Left: 3D-surface representation of the sample A1; Right: level lines.

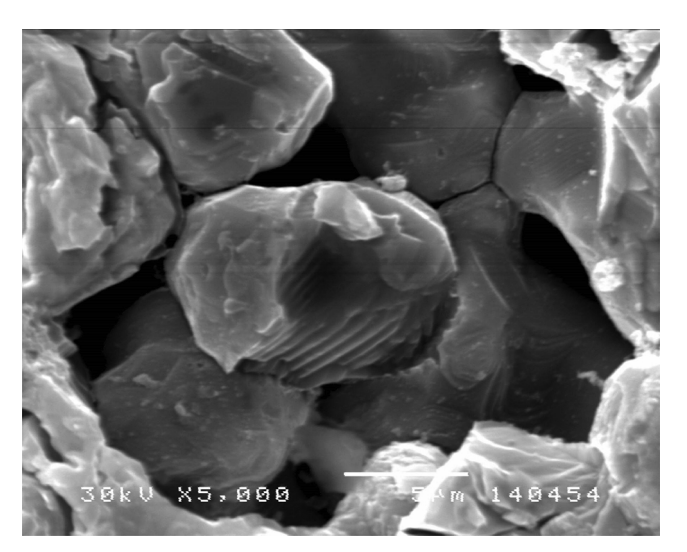


Fig. 13. SEM micrographs of 0.1 wt% Ho doped $\rm BaTiO_3\text{-}ceramic$ sintered at 1380 $^{\circ}\rm C.$

Table 1
The calculated dimensions are summarized in Table 1.

The samples of sintered BaTiO ₃ -ceramic at 120 MPa for 4 hours doped with 0.5 wt%Ho2O3		Fractal dim. DH _f			Average dimension
		1	2	3	difficusion
A	1320 °C	1.7529	1.7499		1.75140
В	1380°C	1.7899	1.7955	1.8025	1.79597

different issues related to the fractal dimensions of the ceramic materials after the sintering process.

3.2. The inner fractality and the α -complex correction

Fractal dimension, typical DH_f , is just slightly above the surface topological dimension, $D_T=2$. The difference $DH_f-D_T=DH_f-2$ is thereby supposed to be responsible for affecting a part of feroelectric phenomena in barium-titanate ceramic that cannot be explained by the purely grain-surface Euclidean geometry. It is suitable to introduce the normalized surface fractality parameter α_S , thus, satisfying the inequality

$$(1 - \varphi) \min \{DH_f - 2\} < \alpha_S < \varphi \max\{DH_f - 2\}, 0 < \varphi < 1$$

which ensures the unit range of $0 < \alpha_S < 1$.

BaTiO₃-ceramic is a porous material that corresponds to lacunar fractal models. It introduces a new phenomenon. Namely, the solidification of porous and "spongy" materials increases overall fractal dimension from (theoretically) 2 to full solid 3. In other words, fractal dimension of a porous material, DH_p satisfies $2 < DH_p < 3$. It causes another correction factor $\alpha_P = D_T - DH_P$, where $D_T = 3$ is dimension of the space and DH_p is the corresponding fractal dimension of a porous configuration. Therefore, $0 < \alpha_P < 1$. The dimensionless quantities α_S and α_P will be called geometric fractality factors.

3.2.1. Temperature involvement

Arguing about the crystal surface "natural roughness" as a macroscopic step collection on the arbitrary crystal plane surface section, the authors hypothesis [24–36] quotes an observation Frenkel [37] had come forward with, that this roughness does not coincide with the crystal faces atomic roughness, with small surface energy, which can occur as a thermal fluctuation consequence at high temperatures. This temperature consideration illustrates impact on dynamic processes within the ceramic body. Such impact generates a motion inside the ceramic crystals in the Fermi gas form, containing different particles such as electrons (Bloch wave), atoms, atomic nuclei, etc.

We suggest the existence of the third factor α_M caused by the influence of disorderly motion of particles, that is, the factor of fractal motion. As it is known, there is a "cloud" of mobile particles in semiconductors (as well as metals) consisting of electrons in atoms with large atomic numbers, nucleons in heavy atomic nuclei, and gases consisting of quasi-particles with half-integral spin called Fermi gas and obeys Fermi-Dirac statistics.

The classic Fermi gas theory assumes that (i) the interactions between the electrons are irrelevant and can be ignored; (ii) the electrons move in a constant potential and we can ignore everything about the structure of the material; (iii) The crystal comprises a fixed background of N identical positively charged nuclei and N electrons, which can move freely inside the crystal without seeing any of the nuclei (monovalent case); and (vi) Coulomb interactions are negligible because the system is overall neutral.

Real Fermi gas dynamics impose the necessity of fractal correction α_M inclusion, that makes the third factor, next to geometric ones α_S and α_P . Since particles have dynamics similar to 3D Brownian one, α_M should be a derivate of Hausdorf fractal dimension DH_M of a Brownian 3D space-filling curve. It is obvious that $1 \leq DH_M \leq 3$. The lower limit, $\min D_M = 1$, is imposed by the continuity of a particle trajectory. The upper limit $\max DH_M = 3$, in turn, is the maximum of trajectory complexity in 3D space. It is reasonable to normalize α_M by taking

V. Mitic, et al.

$$\alpha_M = \frac{1}{2}(DH_M - 1),$$

which gives

$$0 < \alpha_M < 1$$
.

In this way, three independent dimensionless fractality factors α_S , α_P and α_M are introduced. These are real numbers from the open interval (0.1).

Our hypothesis is that the ceramic working temperature must be influenced by these three fractality factors, making the correction of "theoretic" temperature T_f , to get the new "real" temperature T_f , which is temperature affected by the inner fractality of the material $T_f = T - \triangle T$. Obviously, $T_f \leq T$ with the equality of no fractal structure of the S, P, or M type is present.

Now, by setting
$$\alpha = \frac{T_f}{T} = 1 - \frac{\triangle T}{T}$$
, one has

where, α is dependent on all three alpha-components, so,

$$\alpha = \Phi(\alpha_s, \alpha_P, \alpha_M) = u \alpha_s + v \alpha_P + w \alpha_M.$$

where u, v, w > 0 are real coefficients satisfying u + v + w = 1. Now, by the Curie-Weiss law, the relative permittivity will be given

$$\varepsilon_{r,\,\alpha} = \frac{C_c}{T_f - T_S} = \frac{C_c}{\alpha T - T_S} = \frac{C_c}{\Phi(\alpha_s,\,\alpha_P,\,\alpha_M)\ T - T_S},$$

where C_c is the Curie constant.

Although we do not have knowledge of what might be the fractal dimension of the ceramics volume, we can be pretty sure that it is between 2.5 and 3. In manuscripts [23], the authors introduce the formulas for calculating fractal dimension $DH_f(t)$ as the function of sintering time t in three phases, using the Frenkel formula for the sintering initial phase,

$$DH_f(t) = \lim_{\varepsilon \to 0} \frac{\ln\left(N_0(\varepsilon) - \frac{3\pi}{4\varepsilon^3}\left(R_0 - \frac{4\sigma}{3\eta}t\right)^3\right)}{\ln(1/\varepsilon)}$$

Scherer's formula for the intermediate stage

$$DH_{f}(t) = \lim_{\varepsilon \to 0} \frac{\ln \left(N_{0}(\varepsilon) - \frac{4\pi t}{3\varepsilon^{3}} \left(\frac{\gamma n^{1/3}}{\eta} \right) \frac{(\pi - 4\sqrt{2}R_{0})R_{0}^{-2/3}R(t)}{(3\pi - 8\sqrt{2}R_{0})^{2/3}} \right)}{\ln (1/\varepsilon)}$$

and Mackenzie-Shuttleworth for the final stage

$$DH_f(t) = \lim_{\varepsilon \to 0} \frac{\ln\left(N_0(\varepsilon) - \frac{t}{2\varepsilon^3}\left(\frac{4\pi}{3}\right)^{1/3}\left(\frac{\gamma n^{4/3}}{\eta}\right)\left(\frac{1}{\rho} - 1\right)^{2/3}R(t)^3\right)}{\ln\left(1/\varepsilon\right)}$$

where R(t) is the pore radius as a time function. Since this function is decreasing the above formulas, it promises that the limiting value for $DH_f(t)$ at the end of sintering process will be close to 3. Theoretically, $\lim_{t\to\infty}DH_f(t)=3$. This means that intergranular contacts might have dimension much lesser than 3, since it is the substructure of a 3D bulk.

The most important consequence of grain contacts spacious fractal network opens a new viewpoint and the basis for future deeper level of integration, which opens new perspectives to further miniaturization within the electronic properties and functions in ceramic materials and fractal electronics.

Regarding the fact that the previous modern microelectronics development is based on the classic thermodynamic fundamental principles, it is challenging to extend research on these principles based on fractal nature analysis. So, in this paper we open a new approach by introducing fractal corrections in order to open new research perspectives in this field.

Gibbs free energy G is a property that provides a convenient measure of the driving force of a reaction, and it may be used to define

thermodynamic stability. When we want to know whether a process is energetically favorable, we have to determine the change in free energy (ΔG) associated with that process. So for the oxidation processes in ceramic forming, change in free energy is

$$\Delta G = RT \ln p_{O2}$$

In many processes, particularly those that occur in ceramic, there is little, if any, volume change so PV=0. Since the sign of ΔG is dependent on temperature and pressure, a particular system, such as a crystal structure, can be stable only within a certain range of P and T. By varying P and/or T, ΔG eventually becomes negative relative to some other structure and a phase transition occurs. This may be a transition from one aggregate state to another (e.g. during sintering, when we get grain growth and a reduction in the total grain boundary area). Regarding sintering process, as temperature is influenced by fractality factors α_S , α_P , and α_M

$$T_f = \alpha_f T$$
, $\alpha_f = \Phi(\alpha_S, \alpha_P, \alpha_M)$

corrected Gibbs free energy relation is as follows:

$$\Delta G = R\alpha_f T \ln p_{O2}$$

If we take a normalized fractal dimension as the representation of a fractal nature, the individual fractal corrections will be:

$$\begin{split} &\alpha_{S}=\dim\overline{X1}\left(u,\,v\right)\\ &=\dim\sum_{i=1}^{m}\sum_{j=1}^{n}\left(1+R1(\varphi_{i},\,\theta_{j})\right)\left(\sin\varphi\sin\theta\right)\\ &\cos\varphi\sin\theta\\ &\beta_{i}^{\Phi}(\varphi)B_{j}^{\Theta}(\theta)-2,\quad0\leq\alpha_{S}\\ &\leq1\\ &\alpha_{P}=\dim\overline{X2}(u,\,v)\\ &=\dim\sum_{i=1}^{m}\sum_{j=1}^{n}\left(1+R2(\varphi_{i},\,\theta_{j})\right)\left(\sin\varphi\sin\theta\right)\\ &\cos\varphi\sin\theta\\ &\cos\theta\\ &\beta_{i}^{\Phi}(\varphi)B_{j}^{\Theta}(\theta)-2,\quad0\leq\alpha_{P}\\ &\leq1\\ &\alpha_{M}=\dim\overline{X}\left(t\right)=\dim\sum_{i=0}^{n}X(t_{i})B_{i}(t)-1,\quad0\leq\alpha_{M}\leq1 \end{split}$$

We suppose that these fractal corrections α_S , α_P and α_M equally participate in the overall fractal correction α_f i.e.

$$\alpha_{f} = \frac{1}{3}\alpha_{S} + \frac{1}{3}\alpha_{P} + \frac{1}{3}\alpha_{M}$$

$$\alpha_{f} = \frac{1}{3}\left(\dim \sum_{i=1}^{m} \sum_{j=1}^{n} (1 + R1(\varphi_{i}, \theta_{j})) \begin{pmatrix} \sin \varphi \sin \theta \\ \cos \varphi \sin \theta \\ \cos \theta \end{pmatrix} B_{i}^{\Phi}(\varphi)B_{j}^{\Theta}(\theta) - 2\right)$$

$$+ \frac{1}{3}\left(\dim \sum_{i=1}^{m} \sum_{j=1}^{n} (1 + R2(\varphi_{i}, \theta_{j})) \begin{pmatrix} \sin \varphi \sin \theta \\ \cos \varphi \sin \theta \\ \cos \varphi \sin \theta \\ \cos \theta \end{pmatrix} B_{i}^{\Phi}(\varphi)B_{j}^{\Theta}(\theta) - 2\right)$$

$$+ \frac{1}{3}\left(\dim \sum_{i=0}^{n} X(t_{i})B_{i}(t) - 1\right)$$

Obviously $0 \le \alpha_f \le 1$.

4. Conclusion

This scientific paper considers very complex relation between the ceramic material structure, some sintering process phenomena and fractal nature analysis, on one hand, and the energy, on the other hand. Nowadays, that world needs for energy imposed the whole spectra of technological challenges that further reflect on scientific tasks. Our research has been focused on the consolidation of sintering process ceramic material based primarily on Coble's two-sphere model. We extended this model to ellipsoidal Coble's model within the framework

of Euclidian geometry but, because of its limitations, we successfully extended this model by fractal nature recognized in the ceramic structures. Our results confirm, using the quite new understanding of fractal application, the intergranular and pore relations as a supermicro capacitors based on the fractal corrected Heywang model. This new approach treats the intergranular contacts and the intergranular neck as well as the related sintering processes in the light of the fractal nature. This is also very important for energy harvesting and storage on the micro level. In that sense, we successfully introduced fractal correction of temperature as thermodynamic parameter in Gibbs free energy (entropy) equation. From the scientific point of view, this is the first time a relation between the ceramics structure, the extended Coble's sintering process model, the fractal nature, and the energy as inside the structures up to the global level, was established in one paper.

Here, we discuss the role of fractal geometry and the analysis in the field of energy. Some of the early fractal applications have been used as tools in energy research for diverse energy technologies, especially the free energy stock location and conversion as well as the long-term energy storage. In this paper, we left open the possibility of a more flexible, complex, and precise analysis of thermodynamic principles within the microstructure morphology.

So, these intersections are new frontiers in fractal microelectronics that open up new possibilities for further research.

Acknowledgements

This research is a part of the Project "Directed synthesis, structure and properties of multifunctional materials" (172,057). The authors gratefully acknowledge the financial support of the Ministry of Education, Science and Technological Development of the Republic of Serbia for this work.

References

- [1] R.L. Coble, J. Am. Ceram. Soc. 56 (1973) 461-466.
- [2] Michael Barnsley, Fractals Everywhere, Academic Press, Orlando (FL), 1988.
- [3] B. Mandelbrot, The Fractal Geometry of Nature, 3 ed, W. H. Freeman, San Francisco, 1983.
- [4] B. Mandelbrot, Les Objets Fractals, Forme, Hasard Et Dimension, Flammarion, Paris, 1975.
- [5] Falconer Kenneth, The Geometry of Fractal Sets, Cambridge University Press, Cambridge, 1985.
- [6] Falconer Kenneth, Fractal Geometry Mathematical Foundations and Applications, John Wiley & Sons, New York, 1990.
- [7] Michael Frame, Benoit B. Mandelbrot (Eds.), Fractals, Graphics, and Mathematics Education, Mathematical Association of America Inc., 2002.
- [8] M. Harold Hastings, George Sugihara, Fractals. A Users's Guide for the Natural Sciences, Oxford University Press, Oxford, 1993.
- [9] Benoit Mandelbrot, The Fractal Geometry of Nature, W. H. Freeman, New York, 1977.
- [10] R. Massopust, Fractal Peter, Functions, Fractal Surfaces, and Wavelets, Academic Press, New York, 1994.
- [11] Heinz-Otto Peitgen, Hartmut Jurgens, Dietmar Saupe, Chaos and Fractals, New Frontiers of Science, Springer-Verlag, New York, 1992.
- [12] Heinz-Otto Peitgen, H. Richter Peter, The Beauty of Fractals. Images of Complex Dynamical Systems, Springer-Verlag, New York, 1986.
- [13] Claude Tricot, Curves and Fractal Dimension, Springer-Verlag, New York, 1995.
- [14] Mitrovic, V.V. Mitic, $BaTiO_3$ -ceramics electrical model based on intergranular

- contacts, J. Eur. Ceram. Soc. 21 (15) (2001) 2771-2775.
- [15] P. Zheng, J.L. Zhang, Y.Q. Tan, C.L. Wang, Grain-size effects on dielectric and piezoelectric properties of poled BaTiO3 ceramics, Acta Mater. 60 (2012) 5022–5030.
- [16] V.V. Mitić, Lj.M. Kocić, M.M. Ristić, The fractals and BaTiO₃-ceramics sintering, Key Eng. Mater. 136 (1997) 1060–1063.
- [17] V.V. Mitić, P. Petković, Lj. Kocić, BaTiO₃-ceramics capacitance in terms of consolidation parameters, Proc. of Micro Materials Conference and Exhibition Micro Mat97 (1997) 1103–1105. April 16-18.
- [18] V. Mitić, Lj. Živković, Effect of nonstoichiometry on the microstructure and electrical properties of BaTiO3- ceramics, Proc. of the 12th Conference on Glass and Ceramics, Bulgarian Ceramic Society (1997) 479–484 24-26 September 1996.
- [19] B.H. Kaye, A. Random Walk, Through Fractal Dimensions, Wiley-VCH, 1994.
- [20] W. Heywang, H. Thomann, Electronic Ceramics, London and New York, (1991).
- [21] J. Lezanski, W. Rutkowski, Infiltration of a liquid in sintered tungsten, PMI (April) (1987).
- [22] V.V. Mitić, Lj.M. Kocić, M.M. Ristić, The interrelations between fractal and electrical properties of BaTiO3-ceramics, The American Ceramic Society 99th Annual Meeting and Exposition, Cincinnati (1997) 199 May 4-7.
- [23] V.V. Mitić, V. Paunović, J. Purenović, S. Janković, Lj. Kocić, I. Antolović, D. Rančić, The contribution of fractal nature to BaTiO3-ceramics microstructure analysis, Ceram. Int. 38 (2) (2012) 1295–1301.
- [24] V.V. Mitić, Lj.M. Kocić, S. Tidrow, H.J. Fecht, Baldev Raj, Marcel Van, de Vorde, Yashwant Mahajan (Eds.), Structures, Fractals and Energy, Nanotechnology for Energy Sustainability, 2 Vol Wiley-VCH, 2017.
- [25] V. Vuckovic, V.V. Mitic, Lj. Kocic, B. Arizanovic, V. Paunovic, R. Nikolic, Tesla's Fountain - Modeling and simulation in ceramics technology, J. Eur. Ceram. Soc. 38 (8) (2018) 3049–3056.
- [26] V.V. Mitic, Lj. Kocic, V. Paunovic, G. Lazovic, M. Miljkovic, Fractal nature structure reconstruction method in designing microstructure properties, Mater. Res. Bull. 101 (2018) 175–183.
- [27] Z.B. Vosika, V.V. Mitić, G. Lazović, V. Paunović, L. Kocić, Meso-kinetics of one time relaxation electrical processes in BaTiO₃ ceramics—modified Boltzmann-Poisson model, Ferroelectrics 531 (1) (2018) 38–50 27.
- [28] Vojislav V. Mitic, Goran Lazovic, Vesna Paunovic, Sandra Veljkovic, Branislav Randjelovic, Branislav Vlahovic, Hans Fecht, Electronic ceramics fractal microstructure analysis - Minkowski Hull and grain boundaries, J. Ferroelectr. (2015) (accepted for publication).
- [29] V.V. Mitić, I.j.M. Kocić, I.Z. Mitrović, et al., Stojanović (Ed.), Fractals in Ceramic Structure, Proc. of the IX World Round Table Conference on Sintering" Held in Belgrade from 1-4. September 1998: Advanced Science and Technology of Sintering, Kluwer Academic/Plenum Publishers, New York, 1999, pp. 397–402.
- [30] V.V. Mitić, Lj.M. Kocić, I.Z. Mitrović, Fractals and BaTiO₃-ceramics intergranular impedance, Gordon Research Conference: Ceramics, Solid State Studies in Ceramcs, Kimball Union Academy, Meriden (1999) August 1-6.
- [31] V.V. Mitić, Lj.M. Kocić, I.Z. Mitrović, Ceramics dielectric properties in relation with grains surface fractal nature, 102nd Annual Meeting and Exposition of the American Ceramic Society. Abstract Book (2000) 16. April 30 - May 3.
- [32] F. Bastić, D. Sirmić, V.V. Mitić, Lj. Kocić, V. Paunović, S. Janković, M. Miljković, William E. Lee, Rainer Gadow, Vojislav Mitic, Nina Obradovic (Eds.), The Sintering Temperature and the Ho2O3 Concentration Influence on BaTiO₃ Ceramics Microstructure Fractal Nature, Proceedings of the III Advanced Ceramics and Applications Conference, Belgrade (Serbia), Atlantis Press, 201629th Sep.–1st Oct., 2014.
- [33] V.V. Mitić, Lj. Kocić, V. Paunović, F. Bastić, M. Miljković, Fractal nature structure reconstruction analysis method and application in a priori designed microstructure properties prognosis function, IOP Conference Series: Materials Science and Engineering, (2019).
- [34] V.V. Mitic, V. Paunovic, L. Kocic, Fractal approach to BaTiO₃-Ceramics micro-impedances, Ceram. Int. 41 (5) (2015) 6566–6574.
- [35] A. Terzić, Z. Radojević, M. Arsenović, V.V. Mitić, S. Pašalić, Lj. Kocić, Novel application of fractal method in ceramic composites microstructure characterization, Int. J. Appl. Ceram. Technol. 12 (2015) 133–146 br. 1, str..
- [36] V.V. Mitić, V. Paunović, I.j. Kocić, Dielectric properties of BaTiO₃ ceramics and Curie-Weiss and modified Curie-Weiss affected by fractal morphology, in: T. Ohji, M. Singh, S. Mathur (Eds.), Advanced Processing and Manyfacturing Technologies for Nanostructured and Multifunctional Materials, Vol. 35 Ceramic Engineering and Science Proceedings, 2014, pp. 123–133 (6).